Opt Rev (2015) 22:46–51
DOI 10.1007/s10043-015-0049-x

REGULAR PAPER

CFRP damage identification system based on FBG sensors and ELM method

Shizeng Lu · Mingshun Jiang · Lei Jia · Qingmei Sui · Yaozhang Sai

Received: 17 October 2014 / Accepted: 14 November 2014 / Published online: 26 February 2015

Abstract The identification of the damage state of Carbon fiber-reinforced plastic (CFRP) structure is the necessary information for ensuring the safety of CFRP structure. In this paper, the structural damage identification system using fiber Bragg grating (FBG) sensors and the damage identification method were investigated. FBG sensors were used to detect the structural dynamic response signal, which was generated by an active actuation way. Fourier transform and principal component analysis (PCA) were used to extract the damage characteristic. After that, the structural damage identification model was constructed based on extreme learning machine (ELM), whose input is the damage characteristic and output is the damage state. Finally, the damage identification system was established and verified on a CFRP plate with 160 mm $\times$160 mm experiment area. The experimental results showed that the identification accuracy was more than 90 %. This paper provided a reliable method for CFRP structural damage identification.

Keywords Fiber Bragg grating · CFRP structural damage identification · Principal component analysis · Extreme learning machine

1 Introduction

Carbon fiber-reinforced plastic (CFRP) structure has been widely used in aviation applications for its advantages of light quality, high specific strength and stiffness. However, they are very susceptible to the structural damage, such as delamination or matrix cracks, which can reduce the structural stiffness seriously. Besides, the existence of the structural damage can reduce the service time of the structure and lead to catastrophic accidents [1]. Therefore, the structural damage identification is very important for ensuring the structural safety.

The composite structural damage identification can be realized by an active excitation approach, which needs the action of monitored structure and then measurement of resulting response [2]. In traditional, piezoelectric sensors have been wildly used [3, 4]. More recently, fiber Bragg grating (FBG) [5–7] is shown as promising sensors for its advantages of anti-electromagnetic interference, easy to establish sensing network and install without destroying the structures. Capoluongo et al. [8] used FBG sensor technology to detect structural damage, and found that there are minor differences between FBG sensors and conventional sensors. Their research confirmed the excellent performances of FBG to detect damage signals. The structural damage identification can be considered as a pattern recognition problem, whose key points are the extraction of damage characteristic and the selection of recognition algorithm. Pérez et al. [9] and Selva et al. [10] showed that the structural damage can caused the shifts of structural parameters. Therefore, the extraction of damage characteristic by analyzing the structural dynamic response is feasible. The pattern recognition algorithm generally includes neural network and support vector machines. Compared with the neural network, the support vector machines can get a good ability of pattern recognition under small sample [11]. Loutas et al. [12] proposed a pattern recognition scheme for damage diagnosis based on support vector machines, and the scheme was developed and experimentally validated on a composite panel.

S. Lu · M. Jiang (✉) · L. Jia · Q. Sui · Y. Sai
School of Control Science and Engineering, Shandong University, Jinan 250061, Shandong, China
e-mail: jiangmingshun@sdu.edu.cn

However, their performance is affected by the selection of parameters and their model establishment time is much longer. Huang et al. [13, 14] proposed extreme learning machine (ELM) and showed that the ELM has better scalability and achieves similar generalization performance at much faster learning speed than traditional support vector machines. Therefore, the structural damage identification is realized using ELM has a good potential.

The objective of this work is to develop an easy to implement system for CFRP structural damage identification. FBG sensors were pasted on the structural surface to detect the structural dynamic response signal. Fourier transform and principal component analysis (PCA) were used to extract damage characteristic. The ELM, whose input is damage characteristic and output is damage state, was used to realize the structural damage identification. At last, the structural damage identification system was established and verified on a CFRP plate. The experimental results provided a reliable method for CFRP structural damage identification.

2 Experimental setup

2.1 Fundamentals of FBG sensors

FBG is an wavelength modulation optical passive components. According to coupled-mode theory of optical fiber, the Bragg wavelength λ_B can be expressed as follows:

$$\lambda_B = 2n\Lambda \tag{1}$$

where n is fiber grating effective refractive index and Λ is grating period. FBG is sensitive to temperature and strain. Only considering the effect of strain, the relations between FBG wavelength and strain can be expressed as follows:

$$\Delta\lambda_B/\lambda_B = 1 - \left(n^2/2\right)[P_{12} - v(P_{11} + P_{12})]\varepsilon = (1 - P_e)\varepsilon \tag{2}$$

where $\Delta\lambda_B$ is the changes of FBG wavelength, P_{ij} are Pockel's coefficients, v is Poisson's ratio, P_e is effective light function and ε is strain.

Equation (2) shows that there is a linear relationship between the changes of FBG wavelength and strain. When the structure subjected to an impact, the strain produced, and then the FBG wavelength changed. In this way, FBG works as a strain sensor. Therefore, FBG can be used to monitor the structural dynamic response signal.

2.2 Damage identification system

The damage identification system is composed of an optical sensing interrogator (type: SM130 (MOI, USA) with the sampling frequency of 1 kHz), a Computer, a CFRP plate specimen and four FBG sensors. The experiment system and their diagram are shown in Figs. 1 and 2.

The size of CFRP plate is 500 mm × 500 mm × 2 mm and its four edges are clamped on the test bench. On the CFRP plate, 160 mm × 160 mm area was selected as the experimental area. And then, the experimental area was divided into 16 areas and their length and width are both 40 mm. On the surface of the plate, four FBG sensors were stuck on to detect the system dynamic response and their wavelength and location are listed in Table 1.

In this paper, the damage identification method proposed is based on active actuation approach. The active actuation is non-destructive and carried out by a steel ball, whose radius is 8 mm and quality is 25 g, impacting the CFRP plate with the form of free fall. To ensure that the active actuation does not change in each experiment, the impact height should be 250 mm, and the impact area be area 16.

2.3 Damage states

Structural vibration equation can be expressed as the following equation [15]:

$$\boldsymbol{M}\ddot{\boldsymbol{X}} + \boldsymbol{C}\dot{\boldsymbol{X}} + \boldsymbol{K}\boldsymbol{X} = \boldsymbol{P} \tag{3}$$

where $\boldsymbol{M}$ is mass matrix, $\boldsymbol{X}$ is displacement vector, $\boldsymbol{C}$ is damping matrix, $\boldsymbol{K}$ is stiffness matrix and $\boldsymbol{P}$ is external force function. Suppose $\boldsymbol{P} = \boldsymbol{P}(\omega)\exp^{i\omega t}$, and its corresponding response is $\boldsymbol{X} = \boldsymbol{X}(\omega)\exp^{i\omega t}$, where ω is frequency. Equation (3) can be expressed as follows:

$$\boldsymbol{X}(\omega) = \boldsymbol{P}(\omega)/\left(-\omega^2\boldsymbol{M} + i\boldsymbol{C} + \boldsymbol{K}\right). \tag{4}$$

In practice, the overall damping matrix is generally expressed as a linear combination of the overall stiffness matrix and the overall mass matrix. Therefore, the structural damage effect on the damping matrix can be reflected

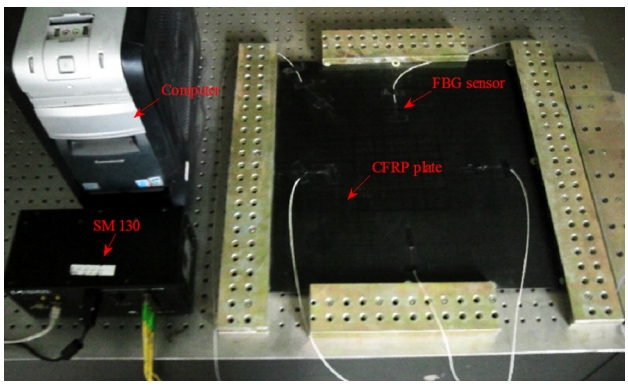

Fig. 1 CFRP damage identification system

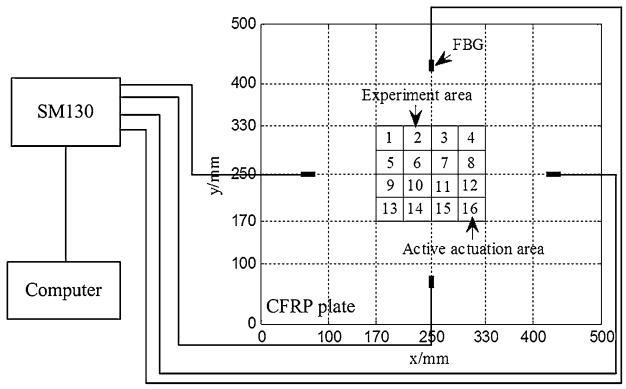

Fig. 2 The diagram of CFRP damage identification system

Table 1 Wavelength of FBG sensor and the paste position

Sensor	Wavelength (nm)	Location (mm)
FBG 1	1531.752	70,250
FBG 2	1536.221	250,70
FBG 3	1539.887	420,250
FBG 4	1565.080	250,420

by a combination of the effect on the stiffness matrix and the mass matrix. Structural damage can decrease the stiffness matrix and has almost no effect on the mass matrix. Therefore, the value of $-\omega^2\boldsymbol{M}+i\boldsymbol{C}+\boldsymbol{K}$ will be decreased. If stiffness matrix invariant and mass matrix increased, the value of $-\omega^2\boldsymbol{M}+i\boldsymbol{C}+\boldsymbol{K}$ will also be decreased. That is to say, the actual damage produces the same result in its dynamic response as responding mass increase produces. In this paper, the structural damage was simulated by adding different lumped masses in 15 different areas, which is shown in Fig. 2. To ensure the same contact area, the base areas are both a round face with diameter of 5cm. Besides, considering the detection capability of FBG and that the changes of structural dynamic response caused by simulated damage can be detected, the lumped mass (125g and 220g) was selected. The different weights of the lumped mass simulated the different damage degrees, and the lumped mass placed on the different areas simulated the different areas. Their corresponding damage states are defined as state 1–31 respectively, as shown in Table 2.

3 Damage characteristic

3.1 Characteristic extraction

The dynamic response signals, in different damage states, were generated by the steel ball impacting the area 16 of the plate. And then, they were detected by FBG sensors. Take FBG 1 signals as an example, which are shown in Fig. 3.

Figure 3 shows that the structural dynamic response were appropriately detected by FBG 1 sensor. However, it was difficult to extract damage characteristic only based on the time domain signals, because they were very similar in shape. Then, Fourier transform was used to obtain their corresponding frequency response. The results are shown in Fig. 4.

By comparing Fig. 4a, b and c, we found that if the structural damage states were different, their frequency responses were different. For example, the amplitude of 109 Hz is 0.0005 nm in state 18 and was larger than 0.0001 nm in state 3. The amplitude of 380 Hz is 0.0001 nm in state 3 and was smaller than 0.0004 nm in state 9. Thus, the signals frequency response can be extracted as damage characteristic.

3.2 Characteristic reduction

The existence of redundant and invalid information leads to the large dimension of damage characteristic. It is necessary to reduce their dimension. Principal component analysis (PCA) [16] is widely used. Defined the signal frequency responses are $\boldsymbol{X}=(\boldsymbol{x}_i,\boldsymbol{x}_i,...,\boldsymbol{x}_m)^T$, where m is the number of training samples and their dimension is p. The covariance matrix $\boldsymbol{C}$ can be obtained:

$$\boldsymbol{C}=\frac{1}{m-1}\sum_{j=1}^{m}(\boldsymbol{x}_j-\overline{\boldsymbol{x}})(\boldsymbol{x}_j-\overline{\boldsymbol{x}})^T \tag{5}$$

where $\overline{\boldsymbol{x}}$ is the mean of $\boldsymbol{x}$. The eigen values λ and its corresponding characteristic vectors $\boldsymbol{U}$ can be obtained from Eq. (5):

$$(\lambda\boldsymbol{I}-\boldsymbol{C})\boldsymbol{U}=\boldsymbol{0} \tag{6}$$

where $\boldsymbol{I}$ is unit matrix. Make $\lambda_1>\lambda_2>\ldots>\lambda_m$, the result of PCA transformation can be expressed as follows:

$$\boldsymbol{Y}=[\boldsymbol{U}_1\quad\boldsymbol{U}_2\quad\ldots\quad\boldsymbol{U}_m]^T\boldsymbol{X}=\boldsymbol{W}^T\boldsymbol{X} \tag{7}$$

where $\boldsymbol{W}$ is transformation matrix and $\boldsymbol{Y}$ is the transform data. The former r row of $\boldsymbol{Y}$ contains the most useful information. The selection of r value has not definite rules. In application, the value of r usually selects from 0.85 to 0.95. To get a higher damage identification accuracy, this paper selects the value of r as 0.95.

$$\sum_{j=1}^{r}\lambda_j\Big/\sum_{j=1}^{m}\lambda_j\geq 0.95 \tag{8}$$

Thus, the p-dimensional damage characteristic is reduced to r-dimensional.

Table 2 The definition of the damage states

State	Definition	State	Definition	State	Definition	State	Definition
1	without damage	9	125 g/area 8	17	220 g/area 1	25	220 g/area 9
2	125 g/area 1	10	125 g/area 9	18	220 g/area 2	26	220 g/area 10
3	125 g/area 2	11	125 g/area 10	19	220 g/area 3	27	220 g/area 11
4	125 g/area 3	12	125 g/area 11	20	220 g/area 4	28	220 g/area 12
5	125 g/area 4	13	125 g/area 12	21	220 g/area 5	29	220 g/area 13
6	125 g/area 5	14	125 g/area 13	22	220 g/area 6	30	220 g/area 14
7	125 g/area 6	15	125 g/area 14	23	220 g/area 7	31	220 g/area 15
8	125 g/area 7	16	125 g/area 15	24	220 g/area 8		

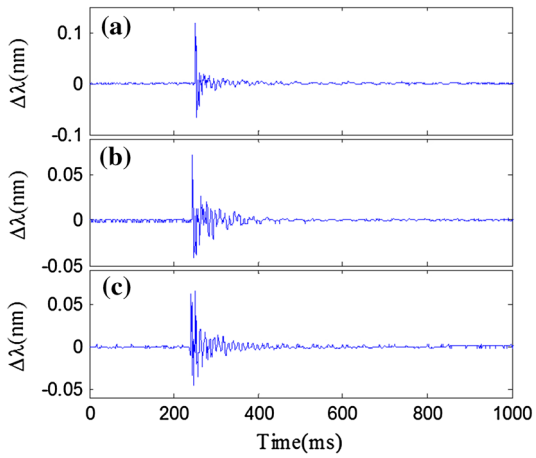

Fig. 3 FBG 1 signals. **a** State 18. **b** State 3. **c** State 9

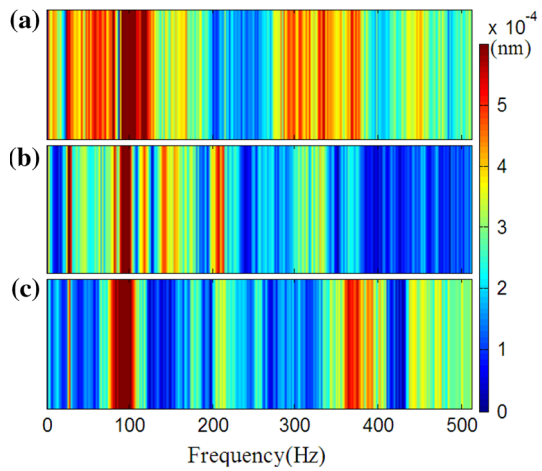

Fig. 4 The results of Fourier transform. **a** State 18. **b** State 3. **c** State 9

4 Damage identification formulation

The essence of structural damage identification is a pattern recognition problem. In this paper, an extreme learning machine (ELM) multi-classification method based on directed acyclic graph (DAG) [17] is used. This method can realize the damage identification by combining several binary ELM classifiers. In this paper, the number of damage state is 15, and $15\times\ (15-1)/2 = 465$ binary ELM classifiers are needed. The establishment process of each binary ELM classifiers is similar. We take the binary ELM classifier, which can identify the damage states 1 and 31, as an example.

Define the training samples are $(\boldsymbol{x}_i, \boldsymbol{y}_i), \boldsymbol{x}_i \in \boldsymbol{R}^r, \boldsymbol{y}_i \in \{1, 31\}, i = 1, 2, \ldots, n$, where $\boldsymbol{x}_i$ is damage characteristic, n is the number of training samples and $\boldsymbol{y}_i$ is the damage state. The function of binary ELM classifier with l hidden layer neurons can be expressed as follows:

$$\sum_{j=1}^{l} \boldsymbol{\beta}_j g(\boldsymbol{w}_j, \boldsymbol{b}_j, \boldsymbol{x}_i) = \boldsymbol{y}_i \tag{9}$$

where $\boldsymbol{w}_j$ is input weight matrix, $\boldsymbol{b}_j$ is the bias term, $\boldsymbol{\beta}_j$ is output weight matrix, and $g(\boldsymbol{w}, \boldsymbol{b}, \boldsymbol{x})$ is a nonlinear piecewise continuous function. The $g(\boldsymbol{w}, \boldsymbol{b}, \boldsymbol{x})$ has many types and sigmoid function type is selected in this paper:

$$g(\boldsymbol{w}, \boldsymbol{b}, \boldsymbol{x}) = 1/[1 + \exp(-(\boldsymbol{w} \times \boldsymbol{x}) + \boldsymbol{b})]. \tag{10}$$

According to any continuous probability distribution, $\boldsymbol{w}_j, \boldsymbol{b}_j$ can be randomly generated. Therefore, the $\boldsymbol{\beta}$ can be obtained as follows:

$$\boldsymbol{\beta} = \boldsymbol{H}^{+}\boldsymbol{Y} \tag{11}$$

where $$\boldsymbol{H} = \begin{bmatrix} g(w_1, b_1, x_1) & \cdots & g(w_l, b_l, x_1) \\ \vdots & \cdots & \vdots \\ g(w_1, b_1, x_n) & \cdots & g(w_l, b_l, x_n) \end{bmatrix}_{n\times l},$$

$\boldsymbol{\beta} = [\beta_1, \ldots, \beta_l]^T_{l\times 2}, \boldsymbol{Y} = [y_1, \ldots, y_r]^T_{n\times 2}$. $\boldsymbol{H}^{+}$ is the Moore–Penrose generalized inverse of matrix $\boldsymbol{H}$. To improve the generalization performance and make the solution more robust, a regularization term c can be introduced to Eq. (11):

$$\boldsymbol{\beta} = \boldsymbol{H}^T \left(\frac{\boldsymbol{I}}{c} + \boldsymbol{H}\boldsymbol{H}^T \right)^{-1} \boldsymbol{Y} \tag{12}$$

Thus, the output function of binary ELM classifier can expressed as follows:

$$f(\boldsymbol{x}) = h(\boldsymbol{x})\boldsymbol{H}^T\left(\frac{\boldsymbol{I}}{C} + \boldsymbol{H}\boldsymbol{H}^T\right)^{-1}\boldsymbol{Y} \tag{13}$$

For a given testing sample, $f(\boldsymbol{x})$ has two values, that is $\{f_1(\boldsymbol{x}), f_2(\boldsymbol{x})\}$, and the identified damage state can be obtained by the following equation:

$$\text{label}(\boldsymbol{x}) = \arg\ \max\ [f_1(\boldsymbol{x}), f_2(\boldsymbol{x})] \tag{14}$$

For this example, if the maximum value is $f_1(\boldsymbol{x})$ then it represents damage state 1, if the maximum value is $f_2(\boldsymbol{x})$ then it represents damage state 31.

When 465 binary ELM classifiers are established, the damage identification based on DAG can be performed, as shown in Fig. 5. For a testing sample, starting at the first binary ELM classifier can identify the states 1 and 31. If the identification result is state 31, the node is exited via the left edge, otherwise, via the right edge. Based on the same process, after 30 identification process, the final damage state can be identified.

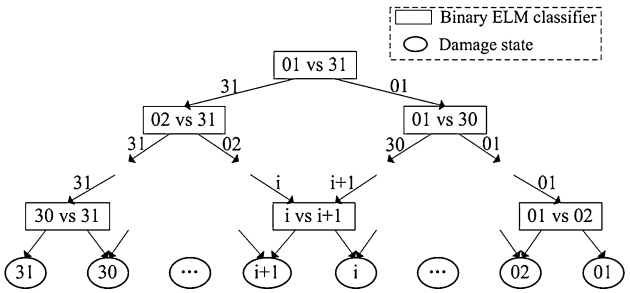

Fig. 5 The damage identification process based on DAG

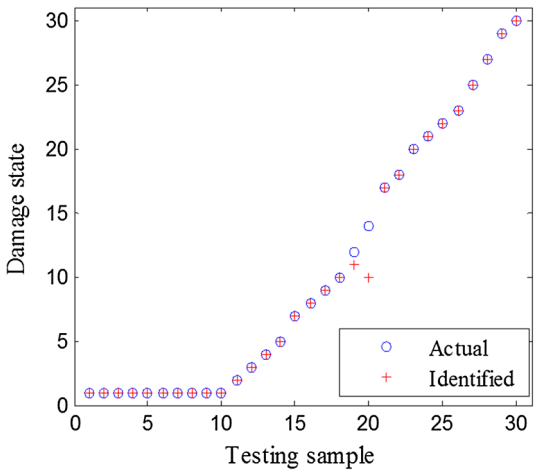

Fig. 6 The identified results of the structural damage state

5 Results and discussion

The damage identification experiments include two parts: the damage identification model training and testing.

5.1 Model training

The experiments were conducted 9 times in damage state 1, and 3 times in each of the remaining 30 damage states. And a total of 99 groups of structural dynamic response signals were detected by FBG sensors.

First, the damage characteristics were extracted by Fourier transform, and their dimension is 2048. Then, PCA was used to reduce their dimension to 66. After that, the finally damage characteristics were set as the training samples to train the damage identification model based on ELM. For ELM, as long as the number of hidden layer nodes is set large enough, the generalization performance of ELM is not sensitive to the number of hidden layer nodes. In this paper, the number of hidden layer nodes was 1000. Besides, the regularization term was 9000. Thus, the ELM model can be trained according to Sect. 4.

5.2 Model testing

After the model trained, another 30 times experiments were conducted, and the damage characteristics were extracted based on Fourier transform and PCA. Then, the damage state was identified based on the trained model. The identified results are shown in Fig. 6. Figure 6 showed that the model made accurate identification 28 times of 30 times experiments. The identification accuracy was more than 90 %. Besides, the computation time of the model testing is shown in Table 3, the software platform using Matlab V.8.1.0.430 and running on the computer with

Table 3 The computation time of model testing

Sample	Time/s	Sample	Time/s	Sample	Time/s	Sample	Time/s	Sample	Time/s
1	0.114	7	0.112	13	0.113	19	0.112	25	0.113
2	0.111	8	0.112	14	0.112	20	0.113	26	0.115
3	0.113	9	0.112	15	0.113	21	0.113	27	0.113
4	0.112	10	0.112	16	0.112	22	0.112	28	0.112
5	0.115	11	0.112	17	0.113	23	0.114	29	0.113
6	0.116	12	0.112	18	0.115	24	0.114	30	0.113

Pentium(R) Dual-Core CPU E6700 and 1.96GB memory. The average computation time was 0.112s, which can meet the practical use requirement. These results confirmed that the proposed damage identification method appropriately functioned in application.

6 Conclusions

In this paper, the CFRP structural damage identification method was researched using FBG sensors. FBG sensors were used to detect the structure dynamic response signal, which contains the damage information. Fourier transform and PCA were used to realize the damage characteristic extraction. After that, the damage identification model based on ELM was build to realize CFRP damage state identification. Finally, this damage identification method was verified on a CFRP plate with the experimental dimensions of 160 mm $\times$ 160 mm. The experimental results showed that the system made accurate identification 28 times of 30 times experiments. The identification accuracy was more than 90 %. This paper provided a reliable method for CFRP structural damage identification.

Acknowledgments This research was supported by the National Natural Science Foundation of China (No. 61174018), Natural Science Foundation of Shandong Province of China (No. ZR2011FQ025) and Fundamental research funds of Shandong University, China (Grant no. 2014YQ009).

References

1. J. Frieden, J. Cugnoni, J. Botsis, T. Gmr, Compos. Struct. **94**, 593 (2012)
2. W.J. Staszewski, S. Mahzan, R. Traynor, Compos. Sci. Technol. **69**, 1678 (2009)
3. I.G. Kim, H.Y. Lee, J.W. Kim, J. Intel. Mat. Syst. Str. **16**, 1007 (2005)
4. M.T.H. Sultan, K. Worden, S.G. Pierce, D. Hickey, W.J. Staszewski, J.M. Dulieu-Barton, A. Hodzic, Mech. Syst. Signal. Pr. **25**, 3135 (2011)
5. S. Takeda, S. Minakuchi, Y. Okabe, N. Takeda, Compos. Part. A. Appl. S. **36**, 903 (2005)
6. B.W. Jang, Y.G. Lee, J.H. Kim, Y.Y. Kim, C.G. Kim, Struct. Control. Health. Monit. **19**, 580 (2012)
7. G. Lu, D. Liang, Y. Xu, Compos. Part. B. Eng. **43**, 594 (2012)
8. P. Capoluongo, C. Ambrosino, S. Campopiano, A. Cutolo, M. Giordano, I. Bovio, L. Lecce, A. Cusano, Sensor. Actuat. A. Phys. **133**, 415 (2007)
9. M.A. Pérez, L. Gil, S. Oller, Compos. Struct. **108**, 267 (2014)
10. P. Selva, O. Cherrier, V. Budinger, F. Lachaud, J. Morlier, Eng. Struct. **56**, 794 (2013)
11. S. Lu, M. Jiang, Q. Sui, Y. Sai, Y. Cao, F. Zhang, L. Jia, Chinese. J. Lasers. **41**, 0305006 (2014). [in Chinese]
12. T.H. Loutas, A. Panopoulou, D. Roulias, V. Kostopoulos, Expert. Syst. Appl. **39**, 8412 (2012)
13. G. Huang, H. Zhou, X. Ding, R. Zhang, T. Lee, Syst. Man. Cy. B. **42**, 513 (2012)
14. G. Huang, D. Wang, Y. Lan, Int. J. Mach. Learn. Cybern. **2**, 107 (2011)
15. J.H. Park, J.T. Kim, D.S. Hong, D.D. Ho, J.H. Yi, J. Sound. Vib. **323**, 451 (2009)
16. W. Huang, H. Yin, Image. Vis. Comput. **30**, 355 (2012)
17. J. Martínez, C. Iglesias, J.M. Matías, J. Taboada, M. Araújo, Appl. Math. Comput. **69**, 1678 (2009)